

Optimization of the Expression of Recombinant Cetuximab Single-Chain Fragment Variable and Comparative its Purification with Magnetic Nanoparticles and Conventional Fast Protein Liquid Chromatography

Masumeh Jalalvand ¹, Khadijeh Falahzadeh ¹, Amirmasoud Jalalvand ²,
Mohammadali Mazloumi ¹, Haleh Bakhshandeh ³, Gholamreza Shahsavari ⁴, Elham Bayat ⁵,
Ziba Veisi Malekshahi ¹, Leila Nematollahi ^{5,*}, Babak Negahdari ^{1,*}

¹ Department of Medical Biotechnology, School of Advanced Technologies in Medicine, Tehran University of Medical Sciences, Tehran, Iran; masumehjalalvand@gmail.com (M.J.); falahzadeh2020@yahoo.com (Kh.F.); m-mazlomi@tums.ac.ir (M.M.); z_vaisemalekshahi@razi.tums.ac.ir (Z.V.M.); b-negahdari@sina.tums.ac.ir (B.N.);

² Department of Biotechnology, School of Medicine, Lorestan University of Medical Sciences, Khorramabad, Iran; amirmasoudjalalvand749@gmail.com (A.M.J.);

³ Department of Nano Biotechnology, New Technology Research Group, Pasteur Institute of Iran, Tehran, Iran; h_bakhshandeh@pasteur.ac.ir (H.B.);

⁴ Department of Biochemistry, School of Medicine, Lorestan University of Medical Sciences, Khorramabad, Iran; reza_shahsavari@yahoo.com (G.S.);

⁵ Biotechnology Research Center, Pasteur Institute of Iran; elhambyat@gmail.com (E.B.); Leila.nematollahi@pasteur.ac.ir (L.N.);

* Correspondence: b-negahdari@sina.tums.ac.ir (B. N.); Leila.nematollahi@pasteur.ac.ir (L.N.);

Scopus Author ID 55918361200

Received: 15.12.2022; Accepted: 23.02.2023; Published: 7.04.2023

Abstract: Various approaches are applied to purify recombinant proteins. Choosing an appropriate purification method seems necessary to achieve a high purity level. In the current study, we compared two different purification strategies, including nickel-nitrilotriacetic acid affinity chromatography using fast protein liquid chromatography system and Ni²⁺-functionalized Fe₃O₄@polydopamine magnetic nanoparticles to purify recombinant cetuximab single-chain fragment variable which specifically attaches to epidermal growth factor receptor according to the affinity interactions between Ni²⁺ and a polyhistidine-tag on the carboxyl-terminus of cetuximab single-chain fragment variable. Epidermal growth factor receptor is overexpressed in many cancer types, especially colorectal cancer cells, making it a valuable candidate for targeted cancer therapy. We optimized expression conditions for recombinant cetuximab single-chain fragment variable in terms of isopropyl-L-thio-β-D-galactopyranoside concentration and cultivation temperature. The soluble cetuximab scFv was extracted from *E. coli* periplasm through osmotic shock. Ni²⁺-functionalized Fe₃O₄@polydopamine magnetic nanoparticles were prepared using the co-precipitation method. Then, nickel-nitrilotriacetic acid affinity chromatography and Ni²⁺-functionalized Fe₃O₄@polydopamine magnetic nanoparticles were employed to purify the cetuximab single-chain fragment variable. Although, according to our experiments, the main strength of nickel-nitrilotriacetic acid affinity chromatography is data reproducibility, this strategy has some big drawbacks, like a sophisticated, costly, and time-consuming purification process. Therefore, compared with nickel-nitrilotriacetic acid affinity chromatography using fast protein liquid chromatography, the Ni²⁺-functionalized Fe₃O₄@polydopamine magnetic nanoparticles technique could be considered a simpler, faster and cheaper method for purification of desired recombinant proteins. Notably, the concentration of purified single-chain fragment variable using Ni²⁺-functionalized Fe₃O₄@polydopamine magnetic nanoparticles gradually decreased in the subsequent batch reactions.

Keywords: single-chain antibodies; magnetic iron oxide nanoparticles; cetuximab; recombinant proteins.

© 2023 by the authors. This article is an open-access article distributed under the terms and conditions of the Creative Commons Attribution (CC BY) license (<https://creativecommons.org/licenses/by/4.0/>).

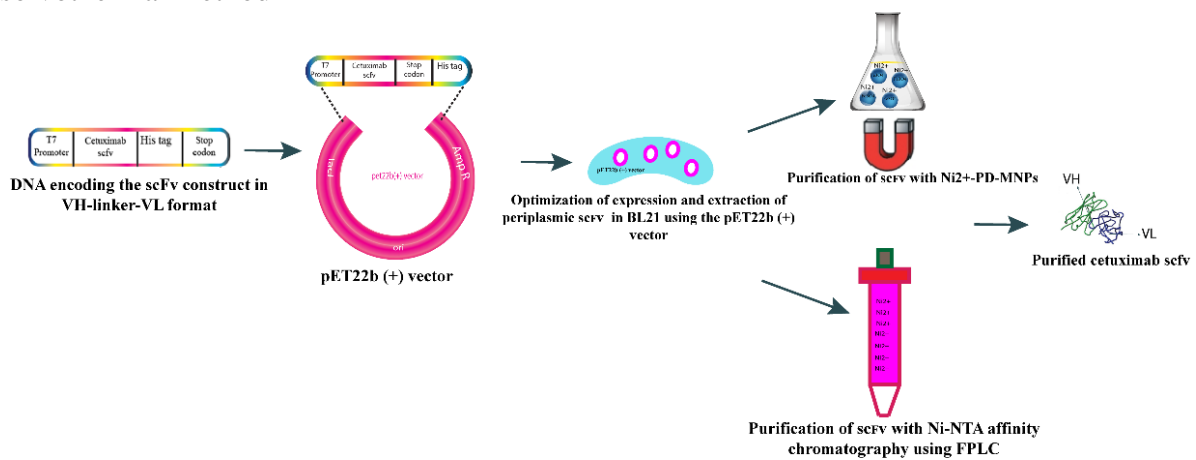
1. Introduction

Antibodies and antibody fragments are widely utilized as therapeutic agents, diagnostic tools, and biosensors, which facilitate the targeted delivery of drugs to a specific location through a carrier system [1]. Single-chain fragment variables (scFv), as a small functional unit of an immunoglobulin molecule, is a heterodimer of the non-covalently linked variable region of immunoglobulin light chain (VL) and the variable region of immunoglobulin heavy chain (VH) domains with a short flexible peptide linker. This linker comprises stretches of Glycine (Gly) and Serine (Ser) residues (Gly₄Ser)₃ and also Glutamic acid (Glu) and Lysine (Lys) residues to improve the flexibility and solubility of scFv, respectively [2-5]. The linker's length and amino acid composition are essential for the native three-dimensional structure and the function of correctly folded proteins [5, 6].

ScFvs, which only include the antigen-binding site, seems preferable to parental antibodies due to their smaller size (~ 30 kDa) with less post-translational modifications, more rapid clearance from circulating blood, better tissue penetration, lower *in vivo* antigenicity response, and less retention in non-target tissues [1, 2, 4]. ScFv fragments have less immunogenicity than whole antibodies while retaining antibody specificity and affinity for the antigen [7]. Compared to conventional antibodies that are produced with costly and time-consuming processes in various mammalian host cells, scFv can be expressed on a large scale in bacterial expression systems with considerably less cost [2, 3, 7]. Furthermore, scFv can be further manipulated and engineered by fusing to diverse moieties like drugs, toxins, cytokines, enzymes, radionuclides, liposomes, and viruses intended for therapeutic purposes such as the treatment of cancers, human immunodeficiency virus (HIV) and neurodegenerative diseases, and also diagnostic imaging and radiotherapy [6, 8]. Due to its favorable features over monoclonal antibodies, notable advancement has been made in expression conditions and purification strategies of scFv [1]. With the high demand for scFv for diagnostic and therapeutic applications, it is vital to optimize its expression conditions and facilitate its purification in order to achieve low-cost and high-yield strategies. Although recombinant histidine-tagged proteins are often purified through affinity chromatography because of this method's high specificity and recovery rate, this procedure is considered a complex and time-consuming technique [9, 10]. These techniques have been proposed for the concentration and purification of intricate biological macromolecules or small molecules. Compared to traditional approaches, new nanoscale materials with remarkable physical and chemical characteristics have been produced [11-14].

Magnetic nanoparticles (MNPs) are appealing nanomaterials due to their biocompatibility, straightforward production process, and capacity to be controlled by an external magnetic field [15-19]. MNPs-based separation techniques have long been understood to be based on the selective adsorption of molecules to certain magnetic particles [20-23]. MNPs are a fantastic alternative for purifying proteins from their natural and lab sources because of their low remanence, low cost, and no negative environmental effects [24-28]. This approach also offers a high rate of operation and accuracy compared to traditional techniques like chromatography and electrophoresis. It does not require sample preparation methods like

centrifugation or filtration [29-31]. This is due to the fact that proteins may be effectively separated and purified using MNPs [17, 32]. Therefore, an alternative system like functionalized MNPs for the purification of these proteins is highly desirable owing to its simple synthesis process and cost-effectiveness [33, 34]. Moreover, using these affinity magnetic materials can effectively shorten the time of histidine-tagged protein purification [35, 36]. Among various functionalized MNPs, Ni²⁺-functionalized Fe₃O₄@polydopamine MNPs (Ni²⁺-PD-MNPs) have been considered a suitable approach for polyhistidine-tagged (His-tagged) protein purification in a protein mixture [37]. Fe₃O₄ nanoparticles have a high surface area, which allows for effective adsorption and, as a result, can promote the adsorption of His-tagged scFv. As a nanomaterial modification coating, polydopamine has several unique adhesion features, such as strong adhesion and high durability. Dopamine's catechol possesses adhesion properties as well. By forming coordination bonds with a wide range of metal ions, such as Ni²⁺, the catechol group might create a complex. The Ni²⁺ could particularly bind to His-tagged scFv, which increases the adsorption of proteins at low protein concentrations. In this study, the expression conditions of scFv were examined further in terms of temperature and isopropyl-L-thio-β-D-galactopyranoside (IPTG) concentration, its periplasmic extraction method was refined, and its interaction with colorectal cancer cells, HCT116, was investigated for the first time. In addition, the present study aimed to compare nickel-nitrilotriacetic acid (Ni-NTA) affinity chromatography using fast protein liquid chromatography (FPLC) and Ni²⁺-PD-MNPs methods to explore the efficiency of these two strategies for purification of cetuximab scFv extracted from osmotic shock fractions (Scheme 1). The iron nanoparticles were also synthesized using the co-precipitation approach, which is easier than the solvothermal method.



Scheme 1. Optimization of the expression of recombinant cetuximab single-chain fragment variable and comparative its purification with magnetic nanoparticles and conventional fast protein liquid chromatography.

2. Materials and Methods

2.1. Production of cetuximab scFv.

To generate soluble scFv, DNA encoding the scFv construct in VH-linker-VL format with standard 15 amino acid linker (Gly₄Ser)₃ containing a hexahistidine affinity tag at the carboxyl-terminus was expressed in BL21 (DE3) *E. coli* strain using the pET22b (+) vector consists of a pelB promoter for controlling periplasmic protein expression [38]. *E. coli* cells were cultured at 37 °C in Luria-Bertani (LB) medium with 100 mg/mL kanamycin in a 150-rpm shaker incubator. For scFv expression, isopropyl-L-thio-β-D-galactopyranoside (IPTG)

was added to a final concentration of 0.8 mM when optical density at 600 nm (OD₆₀₀) reached 0.5 to 0.6 at 30 °C.

2.2. Extraction of periplasmic scFv.

Following IPTG induction, antibody fragments were produced in bacterial periplasmic space, and the cells were harvested 4 h post-induction by centrifugation (9,000 rpm, 15 min, and 4 °C) [39]. Soluble scFv was extracted from *E. coli* periplasm using Tris/EDTA/Sucrose (TES) buffer (30 mM Tris-HCl [pH 8.0], 20%(w/v) sucrose, and 1 mM EDTA) and was incubated on ice for 20 min. In the next step, cell homogenate was separated into the pellet and supernatant by centrifugation (9,000 rpm, 15 min, and 4 °C). The supernatant was discarded after adding 5 mM MgCl₂ to the pellet and incubated on ice for 20 min. Then, it was centrifuged (9,000 rpm, 30 min, and 4 °C) to achieve a clear supernatant containing soluble periplasmic proteins. Following that, the periplasmic fraction was dialyzed against buffered phosphate saline (PBS) for 4 h at 4 °C. After that, the supernatant was removed, and 5 mM MgCl₂ was added, and it was incubated on ice for 20 min. Finally, centrifugal force (9,000 rpm, 30 min, and 4 °C) was applied to achieve a clear supernatant.

2.3. Purification of cetuximab scFv.

His-tagged scFv was purified from the osmotic shock fractions using Ni-NTA affinity chromatography according to the manufacturer's instructions [38]. The periplasmic fraction was loaded at a 1.5 mL/min flow rate on a Ni-NTA column equilibrated with the 10 mM imidazole binding buffer before the purification and attached to an FPLC system (BIORAD). After allowing the sample to flow through, the column was washed with the 20 mM imidazole wash buffer, and the wash fraction was collected for further sodium dodecyl-sulfate polyacrylamide gel electrophoresis (SDS-PAGE) analysis. Following that, purified scFv was recovered with 250 mM imidazole in elution buffer (50 mM NaH₂PO₄, 300 mM NaCl, 250 mM imidazole, pH 8). The purified protein buffer exchange was done against PBS at 4 °C for 4 h. The purity of the scFvs was determined according to standard protocols using SDS-PAGE and confirmed by Western blotting. The purified scFv concentration was determined by Bradford assay using the bovine serum albumin (BSA) as a protein standard.

2.4. Western blotting.

Western blot technique was performed using standard methods [40]. Briefly, after electrophoresis, the cetuximab scFv (20µg/mL) was transferred from gel to a nitrocellulose membrane in a wet blotting system (Denagen Tajhiz). The membrane was blocked with 3% (w/v) BSA in PBS buffer at 4 °C for 16 h (overnight). The membrane was then washed with PBS buffer containing 0.05% tween-20 (PBST) and was incubated with anti-Histidine horseradish peroxidase (HRP) conjugated antibody (1:700 dilution) at room temperature for 2 h. The membrane was washed four times with PBST buffer and one more time with PBS buffer alone. Finally, scFv was detected using 3,3'-diaminobenzidine (DAB)/H₂O₂ system.

2.5. Analysis of antigen binding specificity of scFv by cell-based enzyme-linked immunoassay (ELISA).

Cell-based ELISA was performed to confirm that scFv specifically binds to cell surface epidermal growth factor receptor (EGFR) (Abcam protocol). HCT-116 (human colorectal

carcinoma), A431 (epidermoid carcinoma), and MCF7 (epithelial breast cancer) cell lines (purchased from Pasteur Institute of Iran) were separately seeded in 96-well cell culture plates. After 24 h, cells were harvested and fixed with 100 μ L of 8% paraformaldehyde solution and incubated for 15 min. Then, cells were 3 times washed with PBS. After discarding PBS, 200 μ L of blocking solution was added to each well, and cells were incubated for 2 h. In the next step, the blocking solution was removed, and 100 μ L of purified scFv as primary antibody was added to test wells, and cetuximab antibody as primary antibody solution was added to control wells and incubated overnight at 4 °C which led to the binding of antibodies to the cell surface.

Then, each well was washed three times with 250 μ L wash buffer to remove unbound primary antibodies. After that, 100 μ L of anti-Histidine HRP conjugated antibody (1:250) was added as the secondary antibody to test wells, and 100 μ L of HRP-conjugated anti-mouse IgG antibody (1:500) was added as the secondary antibody to control wells. After 2 h incubation, the secondary antibody solution was discarded, and each well was washed four times with 250 μ L wash buffer. Finally, 3,3',5,5'-Tetramethylbenzidine (TMB) substrate, which reacts with HRP, was added to each plate and was read at 450 nm using Cytation Cell Imaging Multi-Mode Plate Reader

2.6. Synthesis and analytical methods of Ni²⁺-PD-MNPs.

Ni²⁺-PD-MNPs were synthesized via the co-precipitation method [41]. Briefly, 2.97 g iron (III) chloride and 1.193 g iron (II) chloride with a 1:1:0.6 molar ratio were dissolved in 20 ml deionized water. Then, 30 ml 3M NaOH was added dropwise to the above solution until pH 8 was reached, and the solution was stirred for 30 min and heated at 90 °C. The black solid particles, MNPs, were separated by an external magnet and washed several times with deionized water. MNPs (0.2 g) were ultrasonically dispersed in 200 mL of 10 mM Tris-HCl (pH 8.5) for 15 min at 25 °C. Afterward, dopamine hydrochloride (0.2 g) was added to the above solution and stirred at room temperature for 12 h. Then, PD-MNPs were repeatedly washed with water, and PD-MNPs were transferred to 200 mL 100 mM NiSO₄ solution with continuous mechanical stirring at room temperature for 2 h. After magnetic separation, the resultant Ni²⁺-PD-MNPs were stored in deionized water.

The resultant Ni²⁺-PD-MNPs were analyzed by dynamic light scattering (DLS) to determine the particle sizes using Zetasizer NS, Malvern Instrument Ltd, Malvern, UK, at 25.0±0.1 °C. Ni²⁺-PD-MNPs were freshly prepared and diluted with distilled water before measurements. The morphological structure of Ni²⁺-PD-MNPs was studied by scanning electron microscope (SEM). Fourier-transform infrared (FT-IR) is utilized for demonstrating the presence of polydopamine on the MNP's surface. FT-IR spectra were collected on a Nicolet FT-IR spectrometer 4700, USA. Energy dispersive X-ray spectroscopy (EDX) was used to analyze the elemental composition of the synthesized particles. X-ray diffraction (XRD) identification of material phases was carried out with a Rigaku D/MAX 2550 X-ray diffractometer (Rigaku, Japan), using a copper target as the diffraction source and a wavelength of 0.154 nm.

2.7. Purification of cetuximab scFv by Ni²⁺-PD-MNPs.

Ni²⁺-PD-MNPs were used to selectively purify cetuximab scFv from periplasmic solution. 4 ml of Ni²⁺-PD-MNPs were sonicated for 20 min, and 10 ml of a periplasmic solution containing recombinant scFv was added and stirred at room temperature for 30 min. After that,

the Ni²⁺-PD-MNPs were separated by an external magnet. Then, 2 mL of binding buffer containing 10 mM imidazole and 2 mL of binding buffer containing 20 mM imidazole were separately added to Ni²⁺-PD-MNPs in order to remove the non-specifically bounded proteins. Finally, the cetuximab scFv was eluted by the addition of 2 mL of an elution buffer containing 250 mM imidazole. The purity of the recombinant scFv was detected by SDS-PAGE analysis, and also the Bradford protein assay was used to measure the concentration of purified scFv.

3. Results and Discussion

3.1. Polymerase chain reaction (PCR) and digestion.

The correct size of the scFv DNA fragment was confirmed by PCR and restriction analysis. The VH and VL genes were PCR-amplified using specific primers. The PCR product of amplified scFv fragment with the size of approximately 750 bp was visualized on agarose gel (Figure 1a, lane 1). Verification of inserted scFv fragment in the pET22b vector was performed by double digestion with NCOI and XhoI enzymes as shown in (Figure 1b).

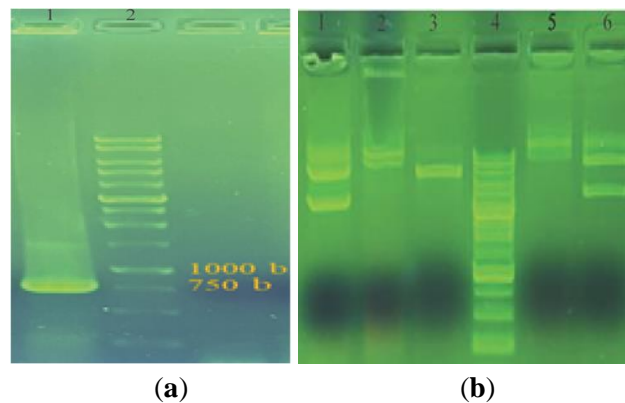


Figure 1. (a) Analysis of PCR product by 1% agarose gel electrophoresis. Lane 1: amplification of scFv DNA fragment; lane 2: DNA marker: (b) Restriction enzyme digestion pattern using NCOI/XhoI was analyzed by 1% agarose gel electrophoresis. Lane 1: undigested pET22b; lane 2: undigested cetuximab; lane 3: cetuximab digested with NCOI/XhoI; lane 4: DNA marker; lane 5: cetuximab digested with NCOI; lane 6: pET22b digested with NCOI.

3.2. Production and optimization and extraction of periplasmic of cetuximab scFv.

BL21 (DE3) *E. coli* strain was transformed with the pET22b (+)/pelB vector containing cetuximab scFv sequence and was subjected to protein expression induction in LB broth medium with 100 mg/mL kanamycin. Therefore, protein expression induction was triggered by the addition of the inducer IPTG. The protein expression condition optimization, including changes in IPTG concentration and growth temperature, was carried out to obtain soluble scFv protein. When the OD at 600 nm reached 0.5 to 0.6 values, the cetuximab scFv expression was induced by various concentrations of IPTG (0.3, 0.4, 0.5, 0.6, 0.8, and 1 mM) and was grown for 4 h. When the optimum IPTG concentration was obtained at 0.8 mM, the expression of scFv protein was carried out at two different temperatures (18 °C and 30 °C). After induction, the bacterial biomass was collected by centrifugation (9,000 rpm for 15 min and 4 °C). In order to perform periplasmic extraction, the cell pellet was resuspended in a TES buffer. A supernatant containing soluble periplasmic scFv was finally achieved, and the total protein was analyzed by SDS-PAGE, followed by Coomassie brilliant blue R250 staining. As shown in Figure 2, the presence of a clear protein band with a molecular weight of around 28 kDa

demonstrated that the recombinant cetuximab scFv was successfully expressed in periplasmic space. According to our results, the final IPTG concentration of 0.8 mM conducted at 30 °C for 4 h was the optimum condition for the high-level expression of soluble cetuximab scFv (red arrow in Figure 2). As shown in Figure 2c, when an empty plasmid that lacks the cetuximab scFv fragment was transferred in the BL21 (DE3) *E. coli* strain, no band appeared as a consequence of protein expression analysis by SDS-PAGE.

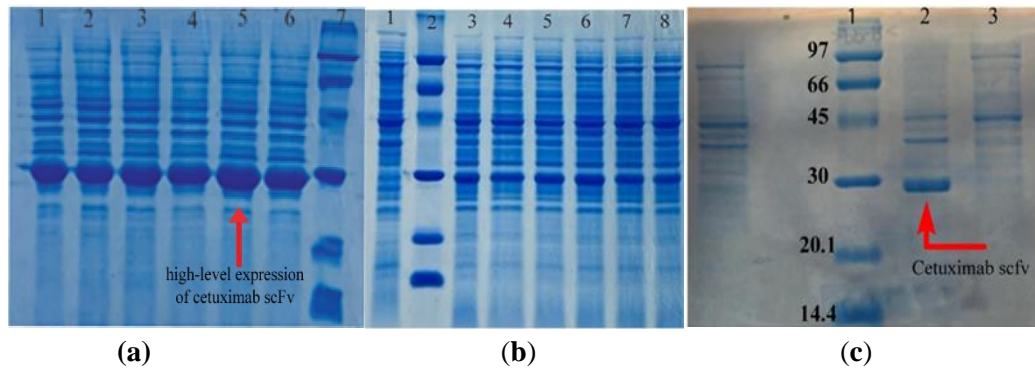


Figure 2. (a) IPTG concentration optimization for soluble cetuximab scFv at 30 °C. Lane 1: 0.3 mM, lane 2: 0.4 mM, lane 3: 0.5 mM, lane 4: 0.6 mM, lane 5: 0.8 mM, lane 6: 1 mM IPTG, and lane 7: protein marker; (b) 15% SDS-PAGE of IPTG-induction optimization of soluble cetuximab scFv at 18 °C. Lane 1: BL21 (DE3) *E. coli* without IPTG induction, lane 2: protein marker, lane 3: 0.3 mM, lane 4: 0.4 mM, lane 5: 0.5 mM, lane 6: 0.6 mM, lane 7: 0.8 mM, lane 8: 1.0 mM IPTG; (c) 15% SDS-PAGE of soluble cetuximab scFv expression at 30 °C. Lane 1: protein marker, lane 2: soluble cetuximab scFv, lane 3: uninduced BL21 (DE3) *E. coli*.

3.3. Western blotting.

After SDS-PAGE analysis, western blotting was performed to detect the cetuximab scFv protein band among cellular protein fractions using an anti-His tag antibody. As demonstrated in Figure 3, the western blotting analysis anti-His tag antibody recognized a single protein band near 28 kDa. Our results confirmed the presence of the cetuximab scFv protein. A 30 kDa protein was used as the positive control to confirm the western blotting results.

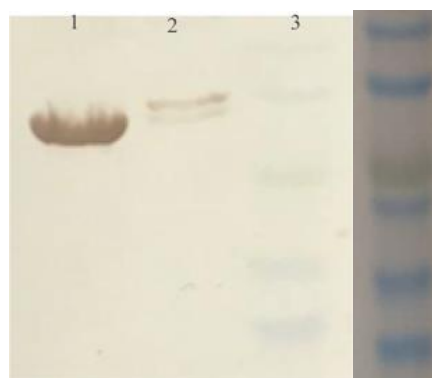


Figure 3. Western blotting analysis using anti-His tag antibody. Lane 1: the detected band for cetuximab scFv, lane 2: positive control, lane 3: protein marker.

3.4. Analysis of antigen binding specificity of scFv by cell-based ELISA.

The cell-based ELISA was employed using the EGFR over-expressing cell lines HCT-116 and A431 (as positive control) and a cell line with low levels of EGFR expression (MCF7) to determine the specificity of the purified cetuximab scFv. As shown in Figure 4, the A431 and HCT-116 cell lines exhibited higher OD values than the MCF7 cell line. Cetuximab scFv

and cetuximab antibody recognized and latched onto the EGF receptor on the surface of the A431 and HCT-116 cell lines, while cetuximab scFv showed reduced attachment to MCF7 cell line due to lower EGFR cell surface levels. Therefore, our results confirmed the high specificity of purified cetuximab scFv for the EGFR antigen.

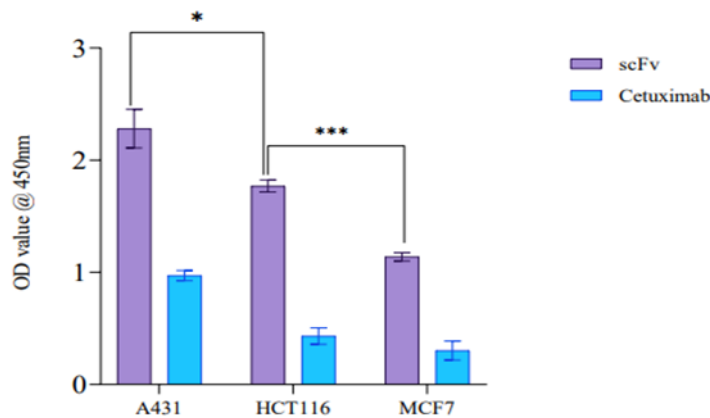


Figure 4. Binding assay of cetuximab scFv by cell-based ELISA. Binding assay of cetuximab scFv by cell-based ELISA. A statistical evaluation was performed using an unpaired t-test. The data displayed are means with standard errors of the means (SEM). *, P value < 0.0467 (compared the interaction of scFv with HCT116 and A-431 cells as indicated); ***, P value < 0.0006 (compared the interaction of scFv and HCT116 with MCF-7 cells as indicated); A P-value below 0.05 was considered statistically significant.

3.5. Purification of cetuximab scFv by FPLC system.

In order to purify desired scFv, it was expressed in 500 mL LB broth media at optimized conditions (0.8 IPTG, 30 °C, 4 h), and periplasmic extraction was carried out. Affinity chromatography was performed using a Ni-NTA column by FPLC system. 20 µg/mL of purified scFv eluted from the FPLC system was obtained from 25 mL total protein solution, and SDS-PAGE analyzed elution fractions. Our findings indicated that non-specific proteins were removed by washing. Coomassie blue staining visualized a single band of cetuximab scFv under the 30 kDa protein marker reference band in the gel. Protein purification outcomes demonstrated that recombinant scFv was successfully purified by the FPLC system (Figure 5).

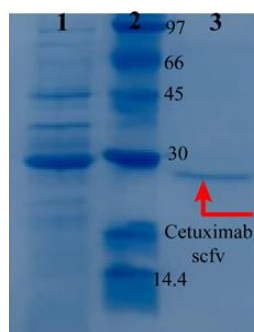


Figure 5. SDS-PAGE analysis of purified cetuximab scFv using Ni-NTA column by FPLC system. Lane 1: initial sample, lane 2: protein marker, lane 3: purified cetuximab scFv.

3.6. Characterization of the Ni²⁺-PD-MNPs.

The Ni²⁺-PD-MNPs dispersions were characterized using DLS. The particle size distribution of Ni²⁺-PD-MNPs is shown in Figure 6a. The average hydrodynamic size of The Ni²⁺-PD-MNPs was 268 nm. SEM showed that the Ni²⁺-PD-MNPs were non-uniform and dispersed, with a diameter of about 50 nm (Figure 6b). The correct polydopamine coating on the surface of MNPs was confirmed by FT-IR spectroscopy (Figure 6c). As observed in the

FT-IR spectrum, the peak between 1500-1650 cm^{-1} indicated N-H stretching vibration, and another peak between 3200-3600 cm^{-1} showed the presence of hydroxyl groups. EDX analysis also confirmed the existence of nickel in the Ni^{2+} -PD-MNPs (Figure 6d). XRD examination of the synthesized materials showed diffraction peaks at 30.1°, 37.1°, 43.1°, 53.4°, 57°, and 62.6° (Figure 6d), which correlate to Fe_3O_4 crystal plane diffraction.

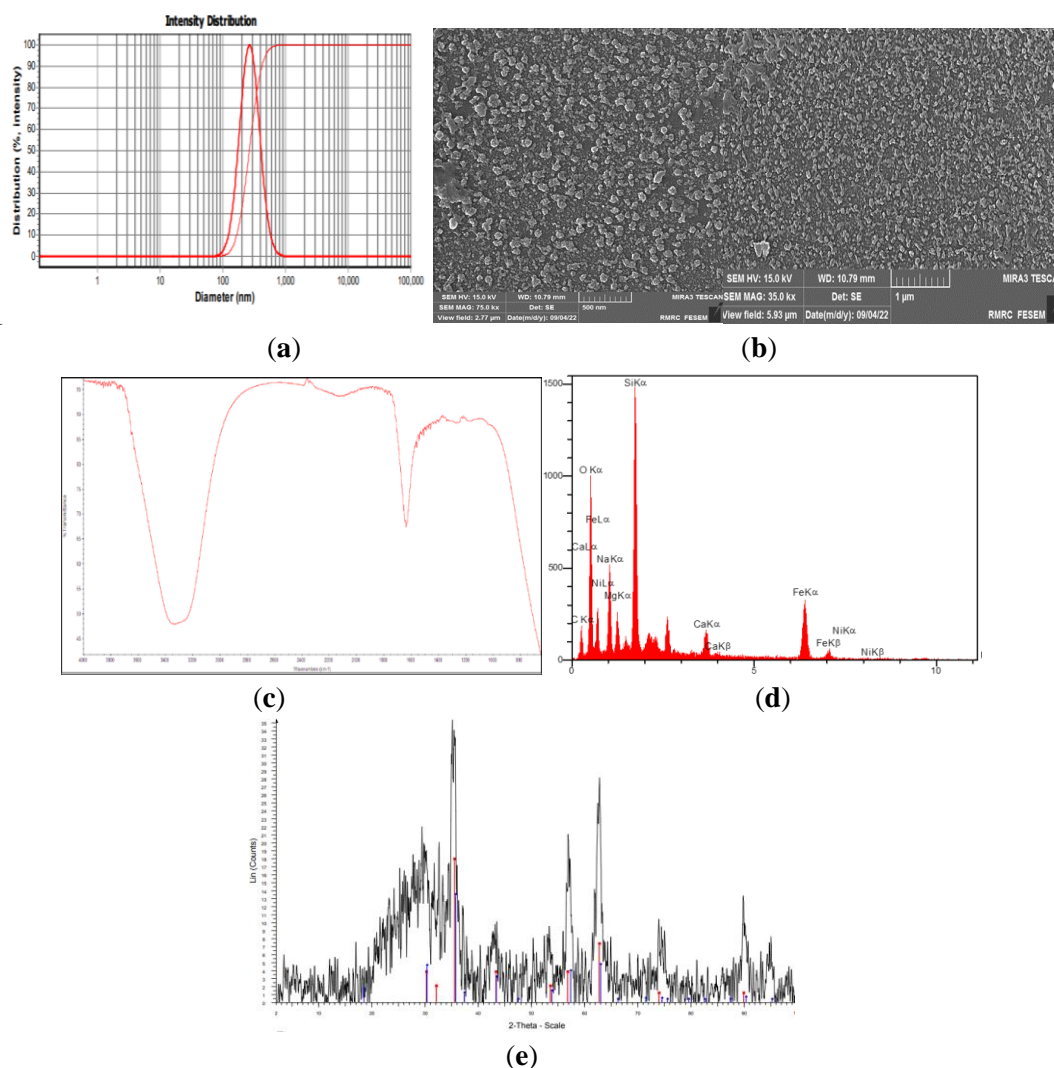


Figure 6. (a) DLS analysis of Ni^{2+} -PD-MNPs; (b) SEM image of Ni^{2+} -PD-MNPs; (c) FT-IR analysis of Ni^{2+} -PD-MNPs revealed that the polydopamine was correctly coated on the surface of MNPs; (d) The dispersive energy X-ray (EDX) analysis of Ni^{2+} -PD-MNPs confirmed the presence of Ni in the prepared nanoparticle; (e) X-ray diffraction of Ni^{2+} -PD-MNPs.

3.7. Purification and reusability of cetuximab scFv by Ni^{2+} -PD-MNPs.

Remarkable progress has been carried out in recombinant protein purification protocols [42-46]. Recombinant protein can be purified using various methods [47-50]. However, purification techniques must be explored for each individual protein based on its application [51]. The broad applications of recombinant proteins in diagnostic and treatment techniques and the vital importance of highly efficient Histidine tagged proteins purification via metal ions like Ni^{2+} highlight the great importance of finding a facile, fast, low-cost, and efficient protein purification strategy [52, 53]. Masthoff *et al.* prepared Fe_2O_3 nanoparticles via solvothermal synthesis using triethylene glycol. Fe_2O_3 nanoparticles were then functionalized with 3-glycidoxypropyltrimethoxysilane and NTA and were charged with Ni^{2+} . This highly specific purification method was used for His-tagged ABF D1.3 scFv. Due to the presence of NTA and

being charged with Ni^{2+} , this system was an alternative approach for the facile and efficient purification of Histagged proteins or peptides [35]. Imani *et al.* used the co-precipitation method to prepare magnetic NiFe_2O_4 nanoparticles. When the Ni was on the surface of NiFe_2O_4 nanoparticles, a suitable system was produced for His-protein isolation. They emphasized that the three-dimensional structure of nickel and iron oxide nanoparticles' distance between nickel and nanoparticles is an important factor in increasing the capacity of NiFe_2O_4 nanoparticles for the purification of His-tag protein [53]. Zeng *et al.* used Ni-MNPs for purification of his-tagged glycoside hydrolase DspB protein. They demonstrated that in comparison with commercial Ni-NTA, their purification system led to more pure and active protein [54].

In an effort to identify an optimal approach for the purification of recombinant proteins, we compared two different purification methods, including Ni-NTA affinity chromatography using the FPLC system and Ni^{2+} -PD-MNPs for the purification of recombinant cetuximab scFv. Due to the binding ability of Histidine-tag to Ni^{2+} , Ni^{2+} -PD-MNPs, and Ni-NTA affinity chromatography could be employed to purify histidine-tagged scFv. Compared to Ni-NTA affinity chromatography using an FPLC system, Ni^{2+} -PD-MNPs were easier to operate. Also, the synthesis process was simpler and more economical for the purification of recombinant cetuximab scFv. The total loaded protein on the Ni-NTA affinity chromatography column was approximately 25 ml, and the concentration of the eluted scFv was 20 $\mu\text{g}/\text{mL}$, whereas the total loaded protein in each batch reaction of Ni^{2+} -PD-MNPs was 10 ml, and the concentration of the eluted scFv was 14 $\mu\text{g}/\text{mL}$ in the first batch reaction.

Purification of cetuximab scFv by Ni^{2+} -PD-MNPs led to identifying a 28kDa clear protein band, in which non-specifically bound proteins were decreased. These findings verified that the Ni^{2+} -PD-MNPs were able to bind and selectively purify the cetuximab scFv (Figure 7a). The concentration of the eluted scFv was determined by Bradford assay [55]. 14 $\mu\text{g}/\text{mL}$ of eluted scFv was obtained from 10 mL total protein in the first batch reaction. We assayed the reproducibility of the Ni^{2+} -PD-MNPs strategy for the purification of cetuximab scFv. To this end, the Ni^{2+} -PD-MNPs were utilized to purify subsequent total protein leading to 9 $\mu\text{g}/\text{mL}$ eluted cetuximab scFv. SDS-PAGE analysis indicated a faint band with a molecular weight of around 28 kDa (Figure 7b).

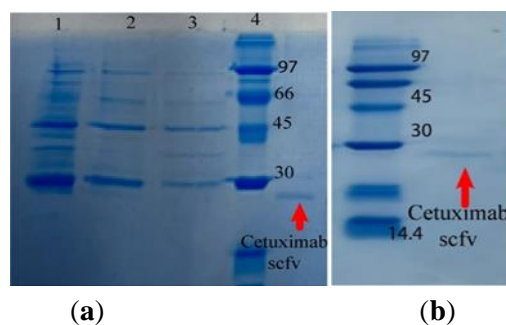


Figure 7. (a) SDS-PAGE analysis of purified cetuximab scFv by Ni^{2+} -PD-MNPs. Lane 1: initial sample, lane 2: binding buffer containing 10 mM imidazole, lane 3: binding buffer containing 20 mM imidazole, lane 4: protein marker, lane 5: purified cetuximab scFv; **(b)** SDS-PAGE analysis of purified cetuximab scFv using Ni^{2+} -PD-MNPs. Lane 1: purified cetuximab scFv, lane 2: protein marker.

4. Conclusions

In this study, the periplasmic extraction method of scFv was optimized, the expression conditions of scFv were further investigated in terms of temperature conditions and IPTG concentration, and its interaction with HCT116 cells, which are colorectal cancer cells, was

examined. Future studies may employ this scFv for the targeted delivery of colorectal cancer because of its association with these cells. On the other hand, two techniques FPLC and nanoparticles were researched to purify it more effectively. Our results demonstrated that the purification capacity of Ni-NTA affinity chromatography for cetuximab scFv remained almost constant after repeated use of the column. Still, the concentration of eluted scFv purified by Ni²⁺-PD-MNPs gradually reduced in the subsequent batch reaction (9 µg/mL) which revealed that the later purification strategy could not be considered as a reproducible method. This may be attributed to the detachment of Ni²⁺ from the nanoparticle surface, which reduces the capacity of Ni²⁺-PD-MNPs for efficient purification of the desired protein. Therefore, we concluded that in comparison with Ni²⁺-PD-MNPs, the FPLC system indicates higher reusability. According to the outcome of this study, we suggest that further research is needed to improve the reproducibility of the Ni²⁺-PD-MNPs purification strategy to achieve a cost-effective and convenient method.

Funding

This project was financially supported by the Tehran University of Medical Sciences and the Pasteur Institute of Iran.

Acknowledgments

The authors would like to thank all who provided deep technical support sincerely.

Conflicts of Interest

The authors have no conflicts of interest to declare that they are relevant to the content of this article.

References

1. Satheeshkumar, P.K. Expression of single chain variable fragment (scFv) molecules in plants: A comprehensive update. *Molecular biotechnology* **2020**, *62*, 151-167, <https://doi.org/10.1007/s12033-020-00241-3>.
2. Ahmad, Z.A.; Yeap, S.K.; Ali, A.M.; Ho, W.Y.; Alitheen, N.B.M.; Hamid, M. scFv antibody: principles and clinical application. *Clinical and developmental immunology* **2012**, *2012*, <https://doi.org/10.1155/2012/980250>.
3. Khantasup, K.; Chantima, W.; Sangma, C.; Poomputsa, K.; Dharakul, T.; Design and generation of humanized single-chain Fv derived from mouse hybridoma for potential targeting application. *Monoclonal Antibodies in Immunodiagnosis and Immunotherapy* **2015**, *34*, 404-417, <https://doi.org/10.1089/mab.2015.0036>.
4. Le, D.T.T.; Dang, L.T.M.; Hoang, N.T.M.; La, H.T.; Nguyen, H.T.M.; Le, H.Q.; Antitumor activity of docetaxel PLGA-PEG nanoparticles with a novel anti-HER2 scFv. *J. Nanomed. Nanotechnol* **2015**, *6*, 1000267, <http://dx.doi.org/10.4172/2157-7439.1000267>.
5. Asaadi, Y.; Jouneghani, F.F.; Janani, S.; Rahbarizadeh, F.; A comprehensive comparison between camelid nanobodies and single chain variable fragments. *Biomarker Research* **2021**, *9*, 1-20, <https://doi.org/10.1186/s40364-021-00332-6>.
6. Monnier, P.P.; Vigouroux, R.J.; Tassew, N.G.; In vivo applications of single chain Fv (variable domain)(scFv) fragments. *Antibodies* **2013**, *2*, 193-208, <https://doi.org/10.3390/antib2020193>.
7. Farajzadeh, D.; Karimi-Gharigh, S.; Jalali-Kondori, P.; Dastmalchi, S. Design and construction of a novel humanized single-chain variable-fragment antibody against the tumor necrosis factor alpha. *Iranian Journal of Pharmaceutical Research: IJPR* **2019**, *18*, 308, <https://www.ncbi.nlm.nih.gov/pmc/articles/PMC6487432/>.
8. Hudson, P.J.; Souriau, C.; Engineered antibodies, *Nature medicine* **2003**, *9*, 129-134, <https://doi.org/10.1038/nm0103-129>.

9. Yang, J.; Ni, K.; Wei, D.; Ren, Y. One-step purification and immobilization of his-tagged protein via Ni²⁺-functionalized Fe₃O₄@ polydopamine magnetic nanoparticles. *Biotechnology and bioprocess engineering* **2015**, *20*, 901-907, <https://doi.org/10.1007/s12257-015-0136-7>.
10. Lichty, J.J.; Malecki, J.L.; Agnew, H.D.; Michelson-Horowitz, D.J.; Tan, S. Comparison of affinity tags for protein purification. *Protein expression and purification* **2005**, *41*, 98-105, <https://doi.org/10.1016/j.pep.2005.01.019>.
11. Eivazzadeh-Keihan, R.; Bahreinizad, H.; Amiri, Z.; Aliabadi, H.A.M.; Salimi-Bani, M.; Nakisa, A.; Davoodi, F.; Tahmasebi, B.; Ahmadpour, F.; Radinekiyan, F.; Maleki, A.; Hamblin, M.R.; Mahdavi, M.; Madanchi, H.; Functionalized magnetic nanoparticles for the separation and purification of proteins and peptides. *TrAC Trends in Analytical Chemistry* **2021**, *141*, 116291, <https://doi.org/10.1016/j.trac.2021.116291>.
12. Alimardani, V.; Abolmaali, S.S.; Yousefi, G.; Nowroozzadeh, M.H.; Tamaddon, A.M. In-situ nanomicelle forming microneedles of poly NIPAAm-b-poly glutamic acid for trans-scleral delivery of dexamethasone. *Journal of Industrial and Engineering Chemistry* **2022**, <https://doi.org/10.1016/j.jiec.2022.11.072>.
13. Borandeh, S.; Alimardani, V.; Abolmaali, S.S.; Seppälä, J. Graphene Family Nanomaterials in Ocular Applications: Physicochemical Properties and Toxicity. *Chemical Research in Toxicology* **2021**, *34*, 1386-1402, <https://doi.org/10.1021/acs.chemrestox.0c00340>.
14. Abedi, M.; Abolmaali, S.S.; Abedanzadeh, M.; Farjadian, F.; Mohammadi Samani, S.; Tamaddon, A.M. Core-Shell Imidazoline-Functionalized Mesoporous Silica Superparamagnetic Hybrid Nanoparticles as a Potential Theranostic Agent for Controlled Delivery of Platinum(II) Compound. *International journal of nanomedicine* **2020**, *15*, 2617-2631, <https://doi.org/10.2147/IJN.S245135>.
15. Zanker, A.A.; Stargardt, P.; Kurzbach, S.C.; Turrina, C.; Mairhofer, J.; Schwaminger, S.P.; Berensmeier, S. Direct capture and selective elution of a secreted polyglutamate-tagged nanobody using bare magnetic nanoparticles. *Biotechnology Journal* **2022**, 2100577, <https://doi.org/10.1002/biot.202100577>.
16. Prados, I.M.; Barrios-Gumiel, A.; de la Mata, F.J.; Marina, M.L.; García, M.C. Magnetic nanoparticles coated with carboxylate-terminated carbosilane dendrons as a reusable and green approach to extract/purify proteins. *Analytical and bioanalytical chemistry* **2022**, *414*, 1677-1689, <https://doi.org/10.1007/s00216-021-03794-7>.
17. Zhao, Y.; Ma, G.; Wang, S. Magnetic Nanoparticle Tracking for One-Step Protein Separation and Binding Kinetics Analysis. *Journal of The Electrochemical Society* **2022**, *169*, 057509, <https://iopscience.iop.org/article/10.1149/1945-7111/ac6bc5>.
18. Lodhi, M.S.; Shaheen, A.; Khan, M.T.; Shafiq, M.I.; Samra, Z.Q.; Wei, D.-Q. A novel method of affinity purification and characterization of polygalacturonase of *Aspergillus flavus* by galacturonic acid engineered magnetic nanoparticle. *Food Chemistry* **2022**, *372*, 131317, <https://doi.org/10.1016/j.foodchem.2021.131317>.
19. Abedi, M.; Abolmaali, S.S.; Abedanzadeh, M.; Borandeh, S.; Samani, S.M.; Tamaddon, A.M.; Citric acid functionalized silane coupling versus post-grafting strategy for dual pH and saline responsive delivery of cisplatin by Fe₃O₄/carboxyl functionalized mesoporous SiO₂ hybrid nanoparticles: A-synthesis, physicochemical and biological characterization. *Materials Science and Engineering: C* **2019**, *104*, 109922, <https://doi.org/10.1016/j.msec.2019.109922>.
20. Niu, C.; Song, X.; Zhang, Y.; Dai, L.; Wei, J.; Yue, T.; Song, Z. A rapid one-step process for the isolation of antibacterial peptides by silica-decorated Fe₃O₄nanoparticles. *LWT* **2022**, *155*, 112858, <https://doi.org/10.1016/j.lwt.2021.112858>.
21. Lu, Y.; Wu, Y.; Hou, X.; Lu, Y.; Meng, H.; Pei, S.; Dai, Z.; Wu, S. Separation and identification of ACE inhibitory peptides from lizard fish proteins hydrolysates by metal affinity-immobilized magnetic liposome. *Protein Expression and Purification* **2022**, *191*, 106027, <https://doi.org/10.1016/j.pep.2021.106027>.
22. Fan, Y.; Yang, Y.; Huang, Y.; Cai, K.; Qiao, Y. Polyamidoamine dendrimer-assisted 3-carboxybenzoboroxole-functionalized magnetic nanoparticles for highly efficient capture of trace cis-diol-containing biomacromolecules. *New Journal of Chemistry* **2022**, *46*, 9889-9896, <https://doi.org/10.1039/D2NJ01242A>.
23. Zhang, J.; Tian, X.; Cui, X.; Zheng, A.; Li, J.; Bai, Y.; Zheng, Y. Facile synthesis of hyperbranched magnetic nanomaterials for selective adsorption of proteins. *Talanta* **2023**, *252*, 123895, <https://doi.org/10.1016/j.talanta.2022.123895>.
24. Kaveh-Baghbaderani, Y.; Allgayer, R.; Schwaminger, S.P.; Fraga-García, P.; Berensmeier, S. Magnetic separation of antibodies with high binding capacity by site-directed immobilization of protein a-domains to bare iron oxide nanoparticles. *ACS Applied Nano Materials* **2021**, *4*, 4956-4963, <https://doi.org/10.1021/acsanm.1c00487>.
25. Weerasuriya, D.R.K.; Bhakta, S.; Hiniduma, K.; Dixit, C.K.; Shen, M.; Tobin, Z.; He, J.; Suib, S.L.; Rusling, J.F. Magnetic nanoparticles with surface nanopockets for highly selective antibody isolation. *ACS Applied Bio Materials* **2021**, *4*, 6157-6166, <https://doi.org/10.1021/acsabm.1c00502>.
26. Tok, K.; Moulahoum, H.; Ghorbanizamani, F.; Harmanci, D.; Balaban Hanoglu, S.; Durmus, C.; Evran, S.; Cicek, C.; Sertoz, R.; Arda, B. Simple workflow to repurpose SARS-CoV-2 swab/serum samples for the isolation of cost-effective antibody/antigens for proteotyping applications and diagnosis. *Analytical and bioanalytical chemistry* **2021**, *413*, 7251-7263, <https://doi.org/10.1007/s00216-021-03654-4>.

27. Çelik, S.Y.; Solak, K.; Mavi, A. Sulfanilamide Modified Magnetic Nanoparticles for Purification of Carbonic Anhydrase from Bovine Blood. *Applied Biochemistry and Biotechnology* **2022**, 1-14, <https://doi.org/10.1007/s12010-022-03983-9>.
28. Krasitskaya, V.V.; Kudryavtsev, A.N.; Yaroslavtsev, R.N.; Velikanov, D.A.; Bayukov, O.A.; Gerasimova, Y.V.; Stolyar, S.V.; Frank, L.A. Starch-Coated Magnetic Iron Oxide Nanoparticles for Affinity Purification of Recombinant Proteins. *International Journal of Molecular Sciences* **2022**, *23*, 5410, <https://doi.org/10.3390/ijms23105410>.
29. Tran, N.; Webster, T.J. Magnetic nanoparticles: biomedical applications and challenges. *Journal of Materials Chemistry* **2010**, *20*, 8760-8767, <https://doi.org/10.1039/C0JM00994F>.
30. Materón, E.M.; Miyazaki, C.M.; Carr, O.; Joshi, N.; Picciani, P.H.; Dalmaschio, C.J.; Davis, F.; Shimizu, F.M. Magnetic nanoparticles in biomedical applications: A review. *Applied Surface Science Advances* **2021**, *6*, 100163, <https://doi.org/10.1016/j.apsadv.2021.100163>.
31. Nithya, R.; Thirunavukkarasu, A.; Sathya, A.B.; Sivashankar, R. Magnetic materials and magnetic separation of dyes from aqueous solutions: a review. *Environmental Chemistry Letters* **2021**, *19*, 1275-1294, <https://doi.org/10.1007/s10311-020-01149-9>.
32. Faraji, M.; Asnaashariifahani, M.; Baharvand, H.; Fard, H.K. Decorated magnetic nanoparticles with polyvinyl alcohol brushes modified with metal chelate affinity groups for purification of proteins. *Biotechnology and Applied Biochemistry* *n/a*, <https://doi.org/10.1002/bab.2378>.
33. Li, P.; Li, M.; Zhang, F.; Wu, M.; Jiang, X.; Ye, B.; Zhao, Z.; Yue, D.; Fan, Q.; Chen, H. High-efficient nucleic acid separation from animal tissue samples via surface modified magnetic nanoparticles. *Separation and Purification Technology* **2021**, *262*, 118348, <https://doi.org/10.1016/j.seppur.2021.118348>.
34. Wang, Z.; Wang, W.; Meng, Z.; Xue, M. Mono-Sized Anion-Exchange Magnetic Microspheres for Protein Adsorption. *International Journal of Molecular Sciences* **2022**, *23*, 4963, <https://doi.org/10.3390/ijms23094963>.
35. Masthoff, I.-C.; David, F.; Wittmann, C.; Garnweitner, G. Functionalization of magnetic nanoparticles with high-binding capacity for affinity separation of therapeutic proteins. *Journal of nanoparticle research* **2014**, *16*, 1-10, <https://doi.org/10.1007/s11051-013-2164-6>.
36. Niu, Y.; Tang, Y.; Gao, R.; Chen, X.; Wang, Y.; Gao, Y.; Zhang, S.; Hussain, S.; Hao, Y.; Wang, S. One-Step Synthesis of Sustainable Montmorillonite-Supported, Copper-Doped Magnetic Nanoparticles for Highly Specific Separation of His-Rich Proteins. *ACS Sustainable Chemistry & Engineering* **2022**, *10*, 5341-5351, <https://doi.org/10.1021/acssuschemeng.2c00749>.
37. Hemalová, K. Metoda izolace His-tag proteinů pomocí TiO₂/Fe₃O₄ s důrazem na čistotu finálního produktu, **2020**, <https://hdl.handle.net/10195/76613>.
38. Sambrook, J.; Russell, D. Cold Spring Harbor Laboratory Press; New York: 2001, *Molecular cloning: a laboratory manual*.
39. Breusted, D.A.; Schönfeld, D.L.; Skerra, A. Comparative ligand-binding analysis of ten human lipocalins. *Biochimica et Biophysica Acta (BBA)-Proteins and Proteomics* **2006**, *1764*, 161-173, <https://doi.org/10.1016/j.bbapap.2005.12.006>.
40. Kurien, B.T.; Scofield, R.H. Western blotting. *Methods* **2006**, *38*, 283-293, <https://doi.org/10.1016/j.ymeth.2005.11.007>.
41. Wang, Y.; Wei, Y.; Gao, P.; Sun, S.; Du, Q.; Wang, Z.; Jiang, Y. Preparation of Fe₃O₄@PMAA@Ni Microspheres towards the Efficient and Selective Enrichment of Histidine-Rich Proteins. *ACS Applied Materials & Interfaces* **2021**, *13*, 11166-11176, <https://doi.org/10.1021/acsaami.0c19734>.
42. Dutta, S.; Bose, K. Protein Purification by Affinity Chromatography, Textbook on Cloning, Expression and Purification of Recombinant Proteins, Springer **2022**, 141-171, https://www.researchgate.net/publication/358125891_Protein_Purification_by_Affinity_Chromatography.
43. Tir, L. Optimization Protocol for Extraction and Purification of Recombinant Protein Modeled with Taq Polymerase, **2022**, <https://our.oakland.edu/handle/10323/11443>.
44. Coskun, K.A.; Yurekli, N.; Abay, E.C.; Tutar, M.; Al, M.; Tutar, Y. Structure-and Design-Based Difficulties in Recombinant Protein Purification in Bacterial Expression, **2022**, <https://doi.org/10.5772/intechopen.103958>.
45. Rahdan, S.; Razavi, S.A.; Nazari, M.; Shojaeian, S.; Shokri, F.; Amiri, M.M.; Ramezani, A.; Zarnani, A.-H. Optimization of Expression and Purification of Recombinant Mouse plac1. *Avicenna Journal of Medical Biotechnology* **2022**, *14*, 61, <http://dx.doi.org/10.18502/ajmb.v14i1.8171>.
46. Mouratou, B.; Pecorari, F. Application of Affitins for Affinity Purification of Proteins. *Affinity Chromatography*, Springer **2022**, pp. 37-48, https://doi.org/10.1007/978-1-0716-2176-9_3.
47. Spiegel, H. Improving recombinant protein recovery from plant tissue using heat precipitation, *Recombinant Proteins in Plants*, Springer **2022**, 147-157, https://doi.org/10.1007/978-1-0716-2241-4_10.
48. Raina, D.; Kumar, V.; Saran, S. A critical review on exploitation of agro-industrial biomass as substrates for the therapeutic microbial enzymes production and implemented protein purification techniques. *Chemosphere* **2022**, 133712, <https://doi.org/10.1016/j.chemosphere.2022.133712>.
49. Matsuda, Y. Current approaches for the purification of antibody–drug conjugates. *Journal of Separation Science* **2022**, *45*, 27-37, <https://doi.org/10.1002/jssc.202100575>.

50. Fox, J.; Scinto, S.; Reagle, T. Affinity Bioorthogonal Chemistry (ABC) Tags for Site-selective Conjugation, On-resin Protein-Protein Coupling, and Purification of Protein Conjugates, **2022**, <https://doi.org/10.1002/anie.202207661>.
51. Structural Genomics Consortium., Architecture et Fonction des Macromolécules Biologiques., Berkeley Structural Genomics Center. *et al.* Protein production and purification, *Nature methods* **2008**, *5*, 135-146, <https://doi.org/10.1038/nmeth.f.202>.
52. Hochuli, E.; Döbeli, H.; Schacher, A. New metal chelate adsorbent selective for proteins and peptides containing neighbouring histidine residues. *Journal of Chromatography A* **1987**, *411*, 177-184, [https://doi.org/10.1016/S0021-9673\(00\)93969-4](https://doi.org/10.1016/S0021-9673(00)93969-4).
53. Imani, S.; Zand, A.; Saadati, M.; Honnari, H.; Maddah, B. Synthetics of NiFe₂O₄ nanoparticles for recombinant His-tag protein purification, **2011**.
54. Zeng, K.; Sun, E.-J.; Liu, Z.-W.; Guo, J.; Yuan, C.; Yang, Y.; Xie, H. Synthesis of magnetic nanoparticles with an IDA or TED modified surface for purification and immobilization of poly-histidine tagged proteins. *RSC advances* **2020**, *10*, 11524-11534, <https://doi.org/10.1039/c9ra10473a>.
55. Ataee, M.H.; Mirhosseini, S.A.; Mirnejad, R.; Rezaie, E.; Hosseini, H.M.; Amani, J. Design of two immunotoxins based rovalpituzumab antibody against DLL3 receptor; a promising potential opportunity. *Research in Pharmaceutical Sciences* **2022**, *17*, 428-444, <https://pubmed.ncbi.nlm.nih.gov/36034078/>.